(Accepted Version of
Delfino et al, Journal of Pharmaceutical and Biomedical Analysis Volume 164, 5 February 2019, Pages 557-573,
https://doi.org/10.1016/j.jpba.2018.11.028,
https://www.sciencedirect.com/science/article/pii/S0731708518321599?via%3Dihub)

X-ray irradiation effects on nuclear and membrane regions of single SH-SY5Y human neuroblastoma cells investigated by Raman micro-spectroscopy

I. Delfino[a], G. Perna[b,c], V. Ricciardi[e,f], M. Lasalvia[b,c], L. Manti[d,e], V. Capozzi[b,c], M. Lepore[e,f,*]

[a]Università della Tuscia, Dipartimento di Scienze Ecologiche e Biologiche, Viterbo, Italy
[b]Università di Foggia, Dipartimento di Medicina Clinica e Sperimentale, Foggia, Italy
[c]Istituto Nazionale di Fisica Nucleare, sezione di Bari, Italy
[d]Università di Napoli "Federico II," Dipartimento di Fisica, Napoli, Italy
[e]Istituto Nazionale di Fisica Nucleare, sezione di Napoli, Italy
[f]Università della Campania "L. Vanvitelli", Dipartimento di Medicina Sperimentale, Napoli, Italy

Abstract.

Raman micro-spectroscopy was performed in vitro on nuclear and membrane regions of single SH-SY5Y human neuroblastoma cells after irradiation by graded X-ray doses (2, 4, 6, 8 Gy). The acquired spectra were analyzed by principal component analysis (PCA) and interval-PCA (i-PCA) methods. Biochemical changes occurring in the different regions of single cells as a consequence of the radiation exposure were observed in cells fixed immediately after the irradiation. The most relevant effects arose from the analysis of the spectra from the cell nucleus region. The observed changes were discussed in terms of the modifications in the cell cycle, resulting in an increase in the DNA-related signal, a protein rearrangement and changes in lipid and carbohydrates profiles within the nucleus. Potential markers of an apoptotic process in cell population irradiated with 6 and 8-Gy X-ray doses could have been singled out. No significant effects were found in spectra from cells fixed 24h after the irradiation, thus suggesting the occurrence of repairing processes of the X-ray induced damage.

Keywords: Raman micro-spectroscopy, single SH-SY5Y human cancer cells, cellular nucleus and membrane, multivariate analysis, X-rays effects on DNA, lipids, proteins and carbohydrates.

*****Maria Lepore**,** E-mail: maria.lepore@unicampania.it

1 Introduction

An estimated 50–60 % of people who develop cancer will be treated at least once with radiotherapy (RT), whose benefits are, by and large, undisputed. To be highly successful, the overall dose administered during an RT treatment must be sufficiently large to inactivate all of the tumor cells, as to achieve local tumor control, yet preserving the surrounding healthy tissue by minimizing or rendering "tolerable" the risk of unacceptably severe late sequelae. Optimizing the effectiveness of radiation therapy is limited, to a great extent, by the variability in radiation response between patients. In fact, probabilities of both normal tissue complication and tumor control depend on individual patient responses to treatment [1]. Improvement of RT strategies relies on accounting for the wide heterogeneity in radiosensitivities displayed by both tumor and healthy cells among patients. RT tailoring requires rapid and accurate prediction of cellular radioresponse. Identifying predictive markers for tumor radioresistance and normal tissue radiosensitivity is currently a primary challenge in clinical radiobiology. The gold standard of radiosensitivity determination is based on the assessment of irradiated cells' colony-forming ability (i.e. the well-known clonogenic assay initially proposed by Puck and Markus [2] over 60 years ago). However, this approach is laborious, as it requires generation from each patient of single cell suspensions from fibroblast (representative of normal cell radiosensitivity) and tumor cell cultures, a particularly demanding task as many cancer cell lines tend to form clumps. Moreover, especially tumor cell lines exhibit usually very low plating efficiencies and, more importantly, may require up to 3 weeks to grow macroscopic colonies. Therefore, surrogate parameters enabling faster and easier prediction of in vitro radiosensitivity are urgently needed. Thus, new alternative approaches have been pursued, as extensively reviewed by Lacombe et al [3].

Advances in this field may, in fact, benefit from the use of non-invasive and fast biochemical methods with the ability to analyze radiation response in vitro or in vivo across a wide variety of biomolecules.

Raman spectroscopy (RS) has been demonstrated to be a valuable tool for providing a non-invasive, label-free, molecular fingerprint of tissues and cells with a high specificity and with no needs of sample treatment or manipulation, also in physiological conditions (i.e. in an aqueous environment). The improvements made in recent years through the development of new methods and approaches for data analysis and pre-processing have considerably increased the relevancy of the information conveyed by the data, facilitating its extraction and use. In particular, multivariate methods, such as the principal component analysis (PCA),

have been demonstrated to be particularly suitable for analyzing Raman spectra from cells and tissues [5].

For these reasons, several researchers have adopted RS and proper data analysis procedures for investigating the effects of X-ray radiation on various kinds of human cells [6-8 and reference therein]. RS has been very fruitful to shed light on outstanding radiobiological issues, such as the variation in patient radiosensitivity [9, 10], the inability to monitor patient's radioresponse during the course of an extended treatment [11, 12], and the failure of current models to predict cell survival or tumor control at single high doses [6,8-10]. In addition, RS has been demonstrated to be useful also for investigating the different radioresponse of various subtypes of breast cancers [11]. Targeted and non-targeted effects in human keratinocytes have been investigated by using RS and PCA analysis by Meade et al [12]. In some cases, significant comparison between the results obtained from RS and conventional biological assays have been also reported [9, 13, 14]. The above-mentioned RS investigations have been performed by using an apparatus equipped with a microscope objective allowing to get information with a high spatial resolution at the microscopic level (micro-RS; μ-RS). In some cases, μ-RS has allowed the examination of the effects of X-ray at the single-cell level [6,7]. For example, human mammary epithelial cells exposed to X-ray radiation at various doses have been investigated at different times after irradiation by PCA analysis on all the available spectral region or in selected intervals (i-PCA) in order to get information embedded in those specific ranges [7].

It is worthwhile noting that the high spatial resolution offered by μ-RS has also allowed the access to sub-cellular information [15-18]. In Ref. 28, regions of cellular cytoplasm, nucleus and nucleoli have been successfully identified thanks to the use of K-means clustering and PCA analysis. Raman signals at sub-cellular level have been also used for visualizing living cells (see Ref. 17 and references therein).

Since ionizing radiation acts in a selective manner on the various biochemical constituents of the cells [19 and reference therein], it can be particularly interesting to investigate the different sub-cellular regions of single cells exposed to X-ray radiation.

In this paper, biochemical and structural changes in the membrane and nucleus regions of single SH-SY5Y neuroblastoma cells following the exposure to graded doses of X-ray were selectively investigated by confocal Raman micro-spectroscopy for the first time to our knowledge. The resulting spectra were analyzed by PCA and i-PCA methods. In particular, Raman investigation was carried out on single normal cells fixed [7, 20-21] immediately after irradiation (t0h-cells) and 24 h after irradiation (t24h-cells) in order to study both the direct

effects of the irradiation and the cellular repair proficiency. The SH-SY5Y neuroblastoma cell line was chosen because it is a human cancer cell line of particular importance in neuroprotection studies to develop new strategies for treatment and/or prevention of central nervous system disorders. Cells were exposed to 2, 4, 6 and 8 Gy doses of X-ray radiation, which are of interest for cancer radiotherapy and radiobiology. In fact, cancer treatment by ionizing radiation typically occurs by administering daily fractions of doses on the order of 2 Gy. The overall treatment may last several weeks with the total dose necessary for local tumor control ranging between 50 and 60 Gy. In addition, these doses are typically used to construct a clonogenic dose-response curve [2]. Raman spectra analysis by i-PCA allowed us to detect subtle variations in the Raman fingerprints of proteins, lipids, and nucleic acids due to X-ray radiation exposure that were discussed in terms of cell-cycle alterations. Particular attention was paid to the comparison of results between t0h-cells and t24h-cells.

2 Materials and Methods

2.1 Materials

DMEM medium, fetal bovine serum, penicillin, L-glutamine, polylysine and formaldehyde were provided by Sigma-Aldrich Co. and used without any further treatments.

SH-SY5Y (American Type Culture Collection, Manassas, VA, USA) is a human cell line subcloned from a bone marrow biopsy taken from a four-year-old female with neuroblastoma; these cells (Fig. 1S) are often used as in vitro models of neuronal function and differentiation.

2.2 Sample Preparation and Treatment

SH-SY5Y cells were cultured in vitro in DMEM medium, supplemented with 20% fetal bovine serum, 1% penicillin and 1% L-glutamine. They were grown at 37°C, 5% CO_2 on polylysine-coated glass coverslips ($22 \times 22 \times 0.17$ mm^3), since polylysine coating is known to favor the adhesion of cells on the glass substrate. The concentration of cells was $\sim 1 \times 10^3$ cells⁄cm^2; at this concentration, cells were not confluent as to leave sufficient intercellular spaces for measurement of the background signal.

A STABILIPLAN machine (Siemens, Munich, Germany) was used for X-ray irradiation. X-rays (250 kVp) were produced by a Thomson tube (TR 300F) and filtered by 1-mm-thick Cu foil. Cellular samples derived from one single batch, in order to avoid interbatch variation.

Cells exposed to various doses of X-rays (2, 4, 6, 8 Gy) at a dose rate of 1.20 Gy⁄ min were investigated together with unexposed cells (0 Gy).

Immediately after X-ray exposure, a set of slides was removed from the growth medium and fixed in 3.7 % paraformaldehyde, in PBS solution for 20 min at room temperature and then briefly washed in distilled water to remove the residue PBS from the surface of the cells. The samples were then stored at 4° C, in fresh fixing solution until analysis (t0h-cells). Another set (maintained in the cell growth medium at 37°C, 5% CO_2) was allowed to recover for 24 h after exposure and then fixed in 3.7% paraformaldehyde (t24h-cells).

After fixation, all the samples were kept in phosphate buffered saline (PBS) solution until Raman measurements were performed.

2.3 Raman micro-spectroscopy measurements

Raman spectra were recorded at room temperature by means of a commercial Raman micro-spectrometer (LabRam, Jobin-Yvon Horiba) equipped with an external Ar+ laser (λ = 514.5 nm). The laser beam was focused on the samples by an Olympus optical microscope with a 100× oil immersion objective (numerical aperture: 1.4); the laser power on the sample was 10 mW. The excitation laser beam, from the immersion objective, passes through the oil drop to the cover glass and was focused on the cell; the laser spot on the focal plane was smaller (about 2 μm) compared to the size of the cell (about 10 μm), hence it was possible to probe a single cell. In order to limit the contribution of the glass substrate to the Raman signal, the excitation laser beam was carefully focused inside the sample. Further details about the apparatus are reported in Ref. 7. The glass coverslip with the cells was placed on the microscope slide provided with a well filled with PBS solution.

The Raman signal was acquired on morphologically intact cells by focusing the laser beam first on the nucleus (visualized by means of a CCD camera), then on the cell membrane and finally on an empty area of the slide close to the cell to record the background spectrum.

2.4 Data Analysis

2.4.1 Preliminary analysis

The whole data set was preliminarily processed to eliminate the contribution of external factors by subtracting from the measured spectrum the background one.

The obtained complex spectra were analyzed in terms of convoluted Lorentzian shaped vibrational modes, by performing a best-fit procedure in order to determine optimized intensity, position, and line-width of Lorentzian peaks, starting from an initial manually set

configuration of the parameters. Peak deconvolution was carried out using the Microcal Origin software (Version 9.0, OriginLab Corporation, Northampton, Massachusetts). The fitting performance was evaluated by means of the $\chi 2$ parameter.

2.4.2 Principal Component Analysis (PCA) and interval-PCA

The fully processed dataset was then analyzed by PCA and i-PCA algorithms [7, 22] in order to represent the dataset by a set of orthogonal eigenvectors separately accounting for most of the variance in the original data. The PCA-based analysis was performed by analyzing the covariance matrix after subtracting the mean of the variables. The number of components to be considered was defined as the one required to explain at least 80% of the total variance. PCA analysis was performed first on the full spectral window (500 to 3200 cm^{-1}), then the spectral window was divided into 15 intervals and the PCA was performed on each interval (i-PCA). These spectral ranges were carefully selected by a proper procedure (500-685, 686-932, 933-1115, 1116-1281, 1282-1357, 1358-1406, 1407-1532, 1533-1585, 1586-1715, 1716-2820, 2821-2905, 2906-3030, 3031-3100, 3101-3163, 3164-3200 cm^{-1}). Firstly, one of the datasets (spectra from the nucleus of t0h-cells) was numerically analyzed to determine the spectral regions with the most significant differences among the spectra, by selecting a reduced set of spectral points or "features". This analysis was performed by using a statistical tool ("rankfeatures") enclosed in the "Bioinformatics Toolbox" of MATLAB® software package (Version 7.6, MathWorks Inc., Natick, Massachusetts). The procedure was described in details in Ref. 23. Briefly, "rankfeatures(X, group)" subroutine allowed us to rank the Raman spectra (X) using an independent evaluation criterion for binary classification in different prefixed "groups". Basically, the program selected 10 points of the spectra (Raman shifts) where the differences between the elements of the two groups are more significant. The comparison among the spectra was performed by grouping them (each group including spectra from cells that had undergone the same irradiation treatment; i.e, no irradiation, irradiation with 2, 4 6 and 8 Gy) and then making the comparison between two groups for each run. At the end of the procedure, a set of spectral points and the width of the intervals were obtained. Among the defined intervals, those in which specific cellular fingerprints are expected to be found were selected and the width of the intervals where optimized to give access to features assigned to DNA/RNA, lipids/carbohydrate, and proteins.

3 Results and Discussion

3.1 Results for t0h-cells

3.1.1 Analysis of the average spectra

The first series of measurements was performed on the not irradiated-SH-SY5Y cell samples adherent to microscope slides. The average spectra obtained for both membrane and nucleus are shown in Fig. 1 (A and B panel, respectively) in the fingerprint region (700-1800 cm^{-1}) and in Fig. 2 (A and B panel, respectively) for the high Raman shift region (HSR) (2800-3200 cm^{-1}). In both the regions, the spectra differ (see Figs. 1C and 2C) according to the obvious difference in the structure and composition of their cellular components. The specific features outlined by the deconvolution procedure are shown in the figures and the main peaks are labelled.

In the fingerprint region, different peaks due to proteins and nucleic acids are clearly visible. In particular, the strong band centered at 1660 cm^{-1} is mainly attributed to the amide I stretching and bending of proteins, with a visible peak generated by the superposition of the contribution of the various secondary structures of proteins (α-helix, β-sheets and random coil) while the peak at ≈1610 cm^{-1} is due to C = C bonds of phenylalanine and tyrosine protein amino acids. The feature at 1575 cm^{-1} is assigned to adenine and guanine nucleobases while the prominent peak at ≈1450 cm^{-1} is due to CH_2/CH_3 bending and scissoring of proteins and lipids, respectively, as well as CH deformation. The peak at 1340 cm^{-1} is due adenine/guanine and to CH_2 twisting and CH deformation while the one at 1309 cm^{-1} is assigned to adenine, amide III and CH_2 twisting. The band at ≈1250 cm^{-1} is assigned to amide III and CH_2 deformation. Different contributes from the protein secondary structure of the amide III band are found (α-helix: mode at 1256 cm^{-1}, β-sheets: at 1248 cm^{-1} and random coil at 1235 cm^{-1}). The peaks at 1204 and 1168 cm^{-1} are assigned to a sum of contributions from tryptophan, tyrosine, phenylalanine amino acids CH bond symmetric stretching and bending. The bands at 1256 and 1297 cm^{-1} are also due to a lipid contribution. The feature at 1123 cm^{-1} is assigned to CN symmetric stretching, CC asymmetric stretching and CO stretching of proteins, lipids and carbohydrates. The peak at 1090 cm^{-1} is mainly due to PO_2^- symmetric stretching vibrations of the phosphodiester nucleic acid backbone with contributions from CC chains stretching of lipids and CO and/or C = C stretching of carbohydrates. The two peaks at around 1030 and 1000 cm^{-1} are assigned to CH in-plane bending and to symmetric ring breathing of phenylalanine. Peaks below 1000 cm^{-1} can be assigned to various contributes: for example to O-P-O backbone and tyrosine (823 cm^{-1}), tryptophan (around 760 cm^{-1}), tyrosine and proline vibrations (around 850 cm^{-1}).

As for the HSR region (2800-3200 cm^{-1}), characteristic bands associated mainly to proteins and lipids are observed. In particular, the shoulders detected at around 2980 and 2940 cm^{-1}

were assigned, respectively, to the asymmetric and symmetric stretching of the methyl groups CH_3 arising from cellular proteins and lipids, and the bands at around 2890 and 2860 cm^{-1} were assigned to the asymmetric and symmetric stretching of the methylene groups of membrane lipids CH_2, respectively.

For the nucleus spectrum the peak at around 1340 cm^{-1} appears prominent, unlike the corresponding peak in the membrane spectrum. This could be ascribed to the contribution due to the nitrogenous DNA bases, showing a possibility for the technique to distinguish between the two cellular regions (see Fig. 1C). A difference in the intensity of the shoulder at ≈2860 cm^{-1}, linked to lipids concentration, is observed in the spectra from membrane and nucleus regions. In fact, this shoulder appears much more noticeable in the membrane spectrum than in the nucleus one, probably due to the contribution given by the membrane phospholipids (see Fig. 2C).

The discussed peaks and relative assignments are reported in Table 1S where information about all the peaks (and relative possible assignments) observed in the complete dataset is reported. The possible assignments are in agreement with Refs. 6, 7, 24-26.

Spectra for membrane and nucleus region obtained from cells fixed immediately after the irradiation (i.e., at t=0) are compared with the control spectrum in Fig. 3 (A and B panel, respectively). As can be clearly seen, each spectrum differs from the others for both the regions, even if the main characteristics, recalling the ones described for the control samples, are observed in all the spectra. To gain a deeper insight into the detected differences, a deconvolution of the spectra of the irradiated cells for membrane and nucleus region has been separately carried out in the two considered spectral regions (700-1800 and 2800-3200 cm^{-1}). Features similar to those obtained for the control spectra were outlined even if shifts in peak positions and changes in peak intensities were observed. The results about the positions of the peaks are summarized in Tables 1 and 2. In particular, in Table 1 the shifts in the peak positions (compared to the position of the corresponding one in the spectrum from the control sample) observed in spectra from the membrane region are reported for the investigated irradiation doses (shifts greater than the spectral resolution are in bold). For the HSR region, significant shifts toward higher Raman wavenumbers appear for the high dose samples (6 and 8 Gy) for all the detected peaks, except for the one located at 2973 cm^{-1} which shows significant shifts also at 2 and 4 Gy doses, but not when a dose of 6 Gy is provided. This can be read as a preliminary indication of modifications in the membrane phospholipids structure. The same behavior is observed in the fingerprint region where positive shifts for quite all the

resolved peaks are observed at high doses (6 and 8 Gy). Shifts towards higher Raman shifts are observed for the phenylalanine-related peak (997 cm^{-1}) and the nitrogenous DNA bases-related peak at 770 cm^{-1} for all doses. Shifts toward lower Raman wavenumber are detected for the 938 cm^{-1}-protein- and carbohydrates-related peak at 2 Gy and toward higher values at 6 Gy.

In Table 2 the shifts in the peak positions (compared to the position of the corresponding peaks detected in the spectrum from the control sample) observed on spectra from the nucleus region are reported for the investigated irradiation doses. In the HSR region, significant shifts toward higher values are observed for the high doses (6 and 8 Gy) for all the detected peaks. The same behavior is observed in the fingerprint region for peaks due to amide I, phenylalanine amino acids, nitrogenous DNA bases and DNA backbones are observed.

These results suggest that X-ray irradiation induced protein rearrangements in the cells and affected DNA and lipids and that information about the details of these effects are embedded in the Raman spectra of the cells [7-10]. In order to extract such an information, PCA and i-PCA analysis was performed taking into account the single spectra.

3.1.2 Principal Component Analysis and i-PCA of single spectra

Results of the PCA analysis on all the datasets of spectra from the membrane and nucleus region of cells fixed immediately after irradiation (t0h-cells) are reported in Figs. 2S and 3S in terms of the loadings and score plots for the first three components (PCs) calculated on the spectra from cells irradiated with the same dose of X-rays. As is evident from Fig. 2S, by taking into account the whole spectra from the membrane region, PCA is not able to get the sources of the subtle variations in the spectra eventually induced by the irradiation treatment. The same happens when the dataset obtained for the nucleus region is considered (see Fig. 3S). This confirms that the main source of variability is the intercellular one that dominates the components obtained considering the full spectra. On the contrary, when the two datasets (nucleus- and membrane-related spectra) are analyzed by using i-PCA, a dependence on the dose of the scores of some components in specific intervals is observed. In the following, the intervals where this dependence was found are discussed along with the significant loadings and Raman features.

3.1.2a i-PCA analysis of spectra from membrane region

As a representative example of i-PCA analysis, in Fig. 4, the results for the 933-1115 cm^{-1} interval are shown in terms of the loadings and the scores for the first three components

(PCs). In the lower panels, the statistical analysis results calculated for the different irradiation doses (0 Gy, 2 Gy, 4 Gy, 6 Gy and 8 Gy) is shown using box plot representation. It is clear that the first component (PC1, accounting for the 97% of the overall variability in the selected spectral range) is quite unfeatured and the corresponding scores do not show any dependence on the dose, thus confirming that also in single intervals the greatest variability is linked to the intrinsic intercellular one. On the contrary, PC3 (accounting for the 0.60% of the dataset variability) shows well defined negative features (located at 1058, and 1098 cm^{-1}) and positive features at 963, and 986 cm^{-1} that can be ascribed to proteins, DNA, lipids and carbohydrates (see Table 1S and Table 3). The dependence of PC3 scores on the dose comes clearly out by the analysis of related panel in Fig. 4. In particular, the PC3 scores decrease with the irradiation dose from highly positive values for the control samples, to slightly lower (positive) values for the samples irradiated with doses of 2 and 4 Gy, down to negative ones for the samples irradiated with a dose of 6 and 8 Gy. This suggests that some relevant changes involving the features observed in the corresponding component occur with higher extension in the spectra from samples irradiated with 6-Gy and 8-Gy doses.

Any spectrum with a higher (i.e., more positive) PC score for a given PC component will have a proportionately higher amount of the positive features and lower amount of the negative features from that component. Therefore, the PC scores can identify changes in the relative biomolecule composition between samples, where the molecular groups responsible for the spectral changes are identified by the features of the corresponding component. Actually, changes in intensities could be rather attributed to changes in overall abundance as well as to shifts in intensity maxima. In the case they are representative of intensity changes, the discussed PC3 score behavior as a function of the dose would suggest a decrease with the dose in the contribution of the positive features and an increase of the negative ones. In particular, since we are looking at the membrane, it is possible to read the results as an indication of the increased contribution from protein-related features at 1000 and 1026 cm^{-1} (phenylalanine symmetric ring breathing and CH in-plane bending), and from lipid-related features at 1058 and 1098 cm^{-1} (CC chain symmetric stretching, CO, C = C str.), along with a decreased contribution from signals at 963 (lipid CH_3 deformation), and 981 cm^{-1} (probably due to protein signal from CC symmetric stretching, β-sheets and CH bending). Similar variations in bands at ≈950, ≈1050, ≈1090 cm^{-1}, have been reported in the literature as an index of increase of glycogen level in cells undergoing survival signaling after exposition to ionizing radiation [8, 9]. The proposed glycogen accumulation has been also confirmed by periodic acid-Schiff staining assay [9].

A similar analysis was carried out for all the intervals previously mentioned. It comes out that the third component shows a dependence of the corresponding score on the dose in the other 5 intervals (namely 1116-1281, 1407-1532, 1586-1715, 2909-3030, and 3031-3100 cm^{-1}). The corresponding score values (and related box plot representation) as a function of the dose are shown in Fig. 5 and the relevant features observed in the corresponding components are reported in Table 3. In the above-mentioned 5 intervals the dependence of the PC3 score on the dose is opposite to the above-discussed one (see Fig. 5a), the score values being highly negative for the control samples, become less negative for samples irradiated with a dose of 2 and 4 Gy and grow to be positive for samples irradiated with high doses (6 and 8 Gy) of X-ray. Accordingly, in all these cases an increased contribution from the positive features of the loadings is suggested along with a decreased contribution from negative features. In particular, an increased contribution is observed for exclusively protein related features at 1178 and 1600 cm^{-1} (phenylalanine/tyrosine CH bending mode and C = C), 1621 cm^{-1} (tyrosine/tryptophan C = C), and to lipid/carbohydrate and protein related features at 1125 (CN symmetric stretching, CC asymmetric stretching, CO stretching), 1259 (Amide III - α-helix and lipid CH_2 deformation), 1460 protein CH_2/CH_3 bending and CH deformation and lipid/carbohydrate CH_2 scissoring and CH deformation), 2950 (CH_3 stretching), and 2972 cm^{-1} (CH_3 stretching) according to Refs. 7-9. A decreasing contribution is suggested for features at 1169 (phenylalanine/tyrosine CH bending mode), 1192 (tryptophan/tyrosine/phenylalanine CH sym. stretching and CH bending), 1219 (Amide III - random coil and lipid CH_2 deformation), 1661 cm^{-1} (mainly Amide I -α-helix, β-sheets, random coil), from CH and CH_3 related modes at 2918 and 3008 cm^{-1} and from the features at 3057 cm^{-1}, related to aromatics.

3.1.2b i-PCA analysis of spectra from nucleus region

More interesting results about the effects of X-ray irradiation on cellular DNA/RNA were obtained by performing the above-described analysis on spectra taken from the nucleus region of the t0h-cells. In fact, PC2 or PC3 scores show a dependence on the dose in a higher number of intervals. Among these intervals, the 686-932 cm^{-1} spectral range is of particular interest because in this range a number of DNA-related features are observed. For this reason, in Fig. 6, the results for this interval are shown in terms of loadings and score values for the first three components. In the lower panels, the statistical analysis results calculated for the different irradiation doses (0 Gy, 2 Gy, 4 Gy, 6 Gy and 8 Gy) are shown using box plot representation. PC3 (accounting for the 0.16% of the dataset variability) shows well defined

negative features (located at 708, 766, and 811 cm^{-1}) and positive features at 722, 784, 824, 851, and 874 cm^{-1} that can be ascribed to proteins, DNA and lipids (see Table 1S and Table 4). The dependence of PC3 scores on the dose comes clearly out by the analysis of the score plots (see Fig. 6, lower panels). In particular, the PC3 scores increase with the irradiation dose from highly negative values for the control samples, to slightly less negative values for the samples irradiate with doses of 2 and 4 Gy, up to highly positive ones for the samples irradiated with a dose of 6 and 8 Gy, thus suggesting that some relevant changes involving the features observed in the corresponding component of the interval occur in the spectra from samples irradiated with 6-Gy and 8-Gy doses.

In the case of the discussed third component (PC3), positive scores are correlated to the variability of specific nucleic acid and protein features, that are different from those that contribute to the negative ones. In particular, it is possible to read the results as an indication of the increased contribution from features at 722 (adenine and choline), 784 (cytosine/thymine/uracil ring breathing), 824 (O-P-O backbone and tyrosine out-of-plane breathing), 851 (tyrosine ring breathing and proline CC stretching), and at 874 cm^{-1} (lipids C_1 - C_2 stretching) and a decreased contribution from bands at 708 (cholesterol), 766 (tryptophan ring breathing), and 811 cm^{-1} (O-P-O stretching RNA and lipids O-P-O stretching).

The results of the same analysis performed on all the other relevant intervals are summarized in Fig. 7 and the relevant features observed in the corresponding components are reported in Table 4. By inspecting Fig. 7, it comes out that in all the intervals except one (panel a) the considered component has score values featuring the same behavior on the dose as the one discussed for the above-discussed PC3 scores of the 686-932 cm^{-1}-spectral region (see the PC3 panel in Fig. 6). In all these cases, the contribution of the negative features observed in the loading plots decreases as the dose increases while the contribution of the positive features increases. The PC3 score value outlined by performing i-PCA in the 933-1115 cm^{-1} interval (results are shown in Fig. 7a) is the only one featuring a different behavior on the dose. In fact, in this case, the PC3 scores decrease with the irradiation dose from highly positive values for the control samples, to slightly lower positive values for the samples irradiated with doses of 2 and 4 Gy, up to highly negative ones for the samples irradiated with a dose of 6 and 8 Gy, thus suggesting that the contribution of the negative features observed increases and that of the positive ones decreases. However, also this behavior suggests that some relevant changes involving the features observed in the loading plot of the third component of the 933-1115 cm^{-1}-interval occur in the spectra from samples irradiated with 6-Gy and 8-Gy doses.

The evidence that the number of intervals where peculiar dose dependence components are found is higher when the nucleus-related dataset is taken into account with respect to when the membrane-related spectra is considered demonstrates that separating spectra from nucleus and membrane can increase the readability of the dose dependence effects and that using spectra from nucleus is more meaningful than using spectra from membrane. In fact, quite all the indication about DNA/RNA-related features are observed only by inspecting the spectra from the nucleus.

By keeping in mind the discussion of previous results, it is possible to say that they suggest an increase in the contribution from quite all the DNA-related features (including single nucleobases, O-P-O and PO_2^- vibrational modes), α-helix-, phenylalanine-, tyrosine-, CH_3 asymmetric stretching (in proteins and lipids)-, lipids C_1-C_2 stretching-related peaks along with a decreased contribution from tryptophan-, β-sheet, CH_3 symmetric stretching (in proteins and lipids)-, CH_3 deformation (in lipids)-, cholesterol-, aromatics (in DNA and lipids)-related peaks according to Refs. 7-10. The 6 Gy-dose X-ray irradiation seems to play a peculiar role. In fact, the significant reduction or increase of the outlined contribute occurs at 6 Gy, thus suggesting that this dose highly changes the ability of the cells to respond to the irradiation stimulus.

These findings are consistent with the reported occurrence of dose-dependent X-ray induced effects on the neuroblastoma cells fixed immediately after the irradiation already observed in other cell lines [6, 27]. For instance, the increase in the α-helix configuration (that occurs in the proteins at the expenses of the β-sheet as a consequence of X-ray irradiation) has been already observed in other cellular systems [6]. Khmaladze [28] has observed specific Raman fingerprints in correspondence of the apoptosis of live central nervous system cells (C6). In particular, he has found that the intensity of the peak at 1165 cm^{-1} increases during the apoptotic cascades, presumably because of the accumulation of proteins and the progression of nuclear condensation. This would also be the reason for the increased DNA-related signal. In addition, the peak at around 1447 cm^{-1} increases in intensity at the beginning of the process. A Raman feature at 1375 cm^{-1} has been observed in Raman spectra from early apoptotic sarcoma cells and the increased intensity in late apoptotic cells has been discussed as an indication of the progression of nuclear condensation [29]. Brauchle et al. have also found that protein peaks (e.g., phenylalanine at 1003 cm^{-1}) increase significantly in necrotic cells [29]. As mentioned for the membrane region results, variations in bands at ≈950, ≈1050, ≈1090 cm^{-1} have been reported as an index of increase of glycogen-level linked to cell survival signaling pathways and cytokines expression. Even though those cytokines are

thought to protect cells against radiation-induced cell death (apoptosis) through regulation of mitochondrial proteins, transcription factors, translation machinery and cell-cycle progression [7] evidence of occurring apoptotic processes in irradiated SH-SY5Y neuroblastoma cells is reported in the literature [30]. In addition, the observed decrease of the contribute at 940 cm^{-1} (which becomes significant always at 6 and 8 Gy-dose irradiation) has been reported in the literature, too, and has been assigned to a cell cycle redistribution and discussed in terms of the glycogen level that correlate positively with the proportion of cells in the G1 phase of the cell cycle and negatively with those in the S and G2/M phases [27]. It is indeed well-known that radiation induces a dose-dependent cell-cycle arrest or slowing down of cells across the cell cycle with an accumulation of damaged cells at the G1/S and G2/M cell-cycle checkpoints, as well as recent works have demonstrated the possibility to detect specific cell-cycle stage radio-sensitivity with μ-RS [13].

Therefore, it is reasonable to hypothesize that the irradiation could have affected the cellular cycle inducing an increase in the proportion of cells blocked at the G2/M phase, resulting in an increase in the DNA-related signal, a protein rearrangement and changes in lipids profiles in the nucleus. In turn, this points to the potential observation by μ-RS of markers of an ongoing apoptotic process in cell population irradiated with 4 and 6 Gy X-ray doses.

3.2 Results for t24h-cells

It is well-known that after irradiation cells undergo reparative processes. In order to investigate the occurrence of these processes, the human neuroblastoma cells fixed after 24 hours (t24h-cells) were also investigated.

3.2.1 Analysis of average spectra

The average spectra for membrane and nucleus of t24h-cells irradiated with all the considered doses are shown in Fig. 8. Similarly to what found for t0h-samples, all the spectra present the same main peaks (labelled in the figure) at all doses with no evident deletions.

The deconvolution procedure performed on the spectra from t24h-cells allowed us to obtain information on the position and intensity of the main peaks for nucleus and membrane regions. In Table 5, the shifts of the peak positions for the membrane region are reported. Differently to what observed for t0h-samples, almost no significant shifts are observed in the HSR region except for one peak (2977 cm^{-1}). Significant shifts are present only for the protein peak at 856 cm^{-1} as well as for DNA peaks at 777 and 813 cm^{-1} for the 2 Gy dose, the

latter peak showing a positive shift also at 6 Gy. The peaks at 1127, 1609 and 2977 cm^{-1} show an increment only when the spectra from 4-Gy irradiated cells are considered.

In Table 6 the shifts of the peak positions for spectra from the nucleus region (calculated with respect to the corresponding features in the control sample) are reported. For nucleus-related spectra differently to what observed for t0h-samples, no significant shifts are observed in the HSR region. The only detected shifts are for very few features: the 933-cm^{-1} band is observed at 939 cm^{-1} when 4-Gy irradiated samples are inspected; the protein-related band located at 1003 cm^{-1} in spectra from the control samples is found at 1008 cm^{-1} in spectra from the 4-Gy irradiated cells; the DNA-related peak at 1053 cm^{-1} is found at 1059 and 1064 cm^{-1} when cells irradiated with 2 and 4 Gy are considered, and the 1126-cm^{-1} band is moved at 1132 cm^{-1} when spectra from 4-Gy irradiated samples are analyzed.

The overall analysis of the Tables 5 and 6 suggests that a very low number of significant shifts are still observed both in the membrane- and nucleus-related spectra when t24h-cells are investigated (in comparison with Tables 1 and 2). This evidence can be read as an effective reduction of the effects of the X-ray as a consequence of the activation of cell repair processes during incubation.

3.2.2 Principal Component Analysis and i-PCA of single spectra

Single spectra obtained from t24h-samples were analyzed by PCA. As for the t0h-samples, the analysis of the overall dataset by taking into account the whole spectrum is not able to identify the origins of the subtle variations in spectra eventually induced by the irradiation treatment neither for nucleus dataset nor for membrane dataset (data are not shown). For the membrane-related spectra, neither by using i-PCA significant differences among the spectra are outlined. On the contrary, if the analysis of nucleus-related spectra is done by using i-PCA, a slight dependence on the dose of the scores of some components is still observed in specific intervals. However, score values with significant differences are found only in three intervals. A synopsis of these results is shown in Table 7 and the score values as a function of the dose are shown in Fig. 9, along with the corresponding box plots. The only detected changes are for features at 1371 (related to thymine), 1572 (adenine and guanine), and 1648 cm^{-1} (Amide I -α-helix, β-sheets, random coil- and lipid/carbohydrate C = C symmetric stretching). In particular, the PC2 score of the loading of the 1358-1406–cm^{-1} range (Fig. 9a) has a negative value for the control samples and positive ones for the irradiated cells, thus meaning that the contribution of the 1371-cm^{-1} (negative) feature is reduced in the spectra from irradiated cells. PC2 scores have almost the same dependence on the dose in both the

1536-1585–cm^{-1} range (where the positive feature at 1572 cm^{-1} is observed in the corresponding loading) and in the 1586-1715-cm^{-1} interval (where the positive feature at 1648 cm^{-1} characterizes the second component loading). They are highly positive for the control samples and have negative values for samples irradiated with 2, 4, 6 and 8 Gy (see Figs. 9b and 9c).

Very few features that depend on the dose were found in the spectra from t24h-cells. This suggests that after 24h quite all the damage due to the X-ray irradiation has been repaired in the neuroblastoma cells. The observed features could be indicative of the presence of residual damage not completely recovered by the repairing processes. Similar evidence of these processes was also observed in our previous work (see Ref. 7) regarding human mammary epithelial cells, but it can be noted that such repair processes appear to be more efficient in SH-SY5Y human neuroblastoma cell lines.

4 Conclusions

By using Raman micro-spectroscopy in combination with i-PCA analysis, the biochemical changes occurring in single neuroblastoma cells as a consequence of cell irradiation with graded X-ray doses were observed by considering cells fixed immediately after the irradiation and by taking into account spectra from cell nucleus region. The observed changes were discussed in terms of the radiation-induced cell-cycle perturbation leading to an increase of the cell accumulating at the G2/M interface, resulting in an increase in the DNA-related signal, a protein rearrangement and changes in lipids and carbohydrates profiles in the nucleus. The potential markers of an apoptotic process in cells irradiated with 6 and 8-Gy X-ray doses were outlined. The observed evidences are no more found in spectra from cells fixed 24h after the irradiation, thus suggesting that after a day the most of the neuroblastoma cells succeeded in repairing the X-ray induced damage. Interestingly, the employed experimental conditions (laser wavelength and power), together with a data collection geometry are compatible with an in vivo study, which would further contribute to clarify interaction processes between cells and ionizing radiation.

Conflict of interest

The authors declare that they have no competing interest.

References

1. Peters L. Radiation therapy tolerance limits—for one or for all? Janeway lecture. Cancer 1996; 77: 2379–85.
2. Puck TT, Marcus PI. Action of x-rays on mammalian cells, J. Exp. Med. 1956; 103: 653-666.
3. Lacombe J et al. Proteomic Approaches to Identify Biomarkers Predictive of Radiotherapy Outcomes. Expert Rev. Proteomics 2013; 10: 33-42.
4. Butler HJ et al., "Using Raman spectroscopy to characterize biological materials. Nat. Protoc. 2016; 11(4): 664–687.
5. Gautam R et al. Review of multidimensional data processing approaches for Raman and infrared spectroscopy. EPJ Techniques and Instrumentation 2015; 2:8 DOI 10.1140/epjti/s40485-015-0018-6
6. Matthews Q et al. Raman spectroscopy of single human tumour cells exposed to ionizing radiation in vivo. Phys. Med. Biol. 2011; 56: 19–38.
7. Delfino I et al. Visible micro-Raman spectroscopy of single human mammary epithelial cells exposed to X-ray radiation. J. Biomed. Opt. 2015; 20(3): 035003 (2015) DOI: 10.1117/1.JBO.20.3.035003.
8. Harder S J et al. A Raman spectroscopic study of cell response to clinical doses of ionizing radiation. App. Spectr. 2015; 69: 193-204.
9. Harder S J et al. Raman spectroscopy identifies radiation response in human non small cell lung cancer xenografts. Sci. Rep. 2016; 6, 21006; doi: 10.1038/srep21006.
10. S. J. Van Nest et al. Raman spectroscopic signatures reveal distinct biochemical and temporal changes in irradiated human breast adenocarcinoma xenografts. Radiation Research 2018; 189: 497-504.
11. P. Meksiarun et al. Breast cancer subtype specific biochemical responses to radiation. Analyst 2018; 143: 3850-3858.
12. Meade A D et al. Vibrational spectroscopy in sensing radiobiological effects: analyses of targeted and non-targeted effects in human keratinocytes. Faraday Discuss. 2016; 187: 213-234.

13. Meade A. D. et al. Prediction of DNA damage and G2 chromosomal radio-sensitivity ex vivo in peripheral blood mononuclear cells with label-free Raman microspectroscopy. International Journal of Radiation Biology, 2018; DOI: 10.1080/09553002.2018.1451006.
14. Maguire A et al. Analyses of ionizing radiation effects in vitro in peripheral blood lymphocytes with Raman spectroscopy. Radiation Research 2015: 183: 407–416.
15. Bonnier F, Byrne H J. Understanding the molecular information contained in principal component analysis of vibrational spectra of biological systems. Analyst 2012; 137: 322-332; doi:10.1039/c1an15821j.
16. Prats Mateu B et al. Label-free live cell imaging by confocal Raman microscopy identifies CHO host and producer cell lines. Biotechnol. J. 2017; 12: 1600037 DOI: 10.1002/biot.201600037.
17. Kann B et al. Raman microscopy for cellular investigations — From single cell imaging to drug carrier uptake visualization. Advanc. Drug Delivery Rev. 2015; 89: 71–90.
18. Byrne H J et al. Advancing Raman microspectroscopy for cellular and subcellular analysis: towards in vitro high-content spectralomic analysis. App. Opt. 2018; 57(22), E11-E19, DOI: 10.1364/AO.57.000E11.
19. Baskar R et al. Biological response of cancer cells to radiation treatment. Front. Molec. Biosci. 2014; 1, art. no. 24, 1-9.
20. Harvey T J et al. Classification of fixed urological cells using Raman tweezers. J. Biophotonics 2009; 2(1–2): 47–69.
21. Meade A D, Byrne H J, Lyng F M. Spectroscopic and chemometric approaches to radiobiological analyses. Mutation Research/Reviews in Mutation Research 2010; 704(1): 108-114.
22. Leardl L, Nørgaard L. Sequential application of backward interval partial least squares and genetic algorithms for the selection of relevant spectral regions. J. Chemom. 2004; 18: 486–497.
23. d'Apuzzo F et al. Monitoring early phases of orthodontic treatment by means of Raman spectroscopies. J. Biomed. Opt. 2017 22(11) art.n. 115001 (11 pages). DOI: 10.1117/1.JBO.22.11.115001.
24. Ong Y H, Lim M, Liu Q. Comparison of principal component analysis and biochemical component analysis in Raman spectroscopy for the discrimination of apoptosis and necrosis in K562 leukemia cells. Opt. Express 2012; 20(20): 22158–22171.
25. Meade A D et al. Studies of chemical fixation effects in human cell lines using Raman microspectroscopy. Analyt. Bioanalyt. Chem. 2010; 396(5): 1781-1791.

26. Notingher I et al. In situ characterisation of living cells by Raman spectroscopy. J. Spectrosc. 2002; 16(2): 43-51.
27. Schulze H G et al. Raman Microscopy of Human Embryonic Stem Cells Exposed to Heat and Cold Stress. Appl. Spectr. 2011; 65(12): 1380-1386.
28. Khmaladze A. Examining live cell cultures during apoptosis by digital holographic phase imaging and Raman spectroscopy. J. Phys.: Conf. Ser. 909, art. no. 012001 (2017) doi: 10.1088/1742-6596/909/1/012001.
29. Brauchle E et al. Cell death stages in single apoptotic and necrotic cells monitored by Raman Microspectroscopy. Sci. Rep. 2014; 4, art.no. 4698 (9 pages) DOI: 0.1038/srep04698.
30. S. Kim et al. Inhibition of gamma ray-induced apoptosis by stimulatory heterotrimeric GTP binding protein involves Bcl-xL down-regulation in SH-SY5Y human neuroblastoma cells. Experimental and Molecular Medicine 2007; 39(5): 583-593.

FIGURES

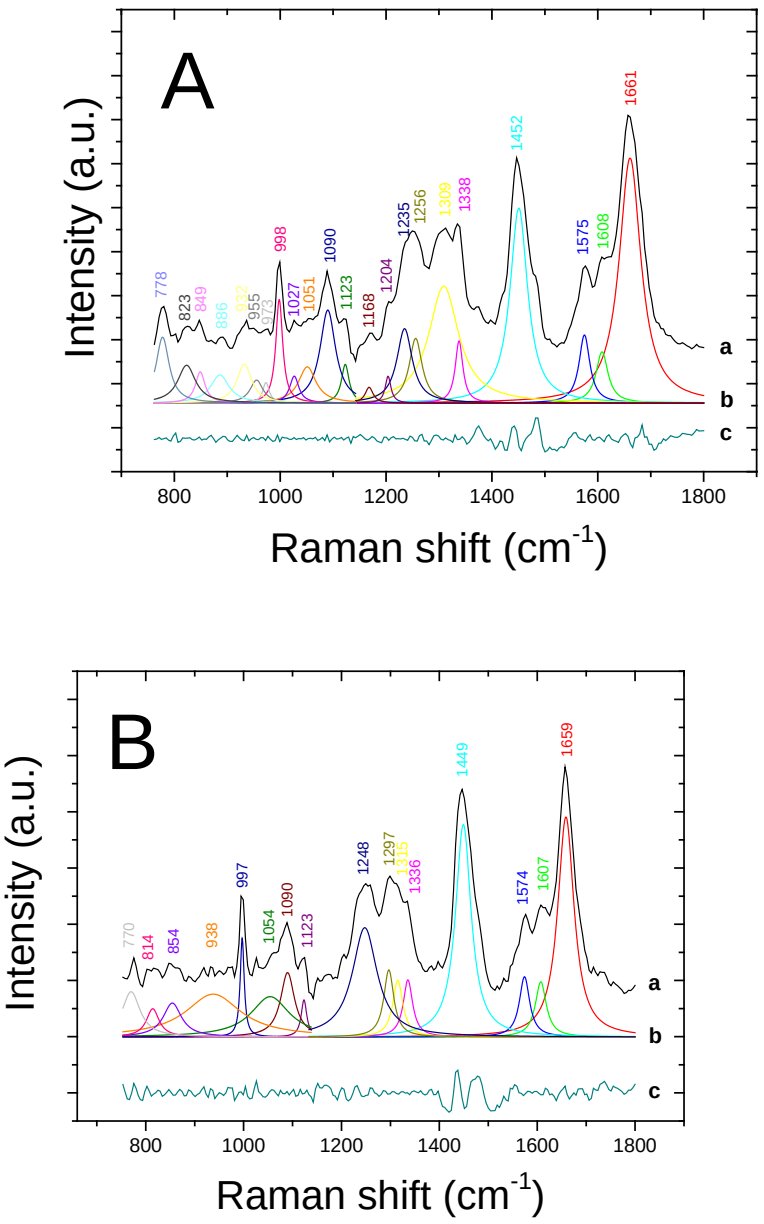

Fig. 1 (cont'd)

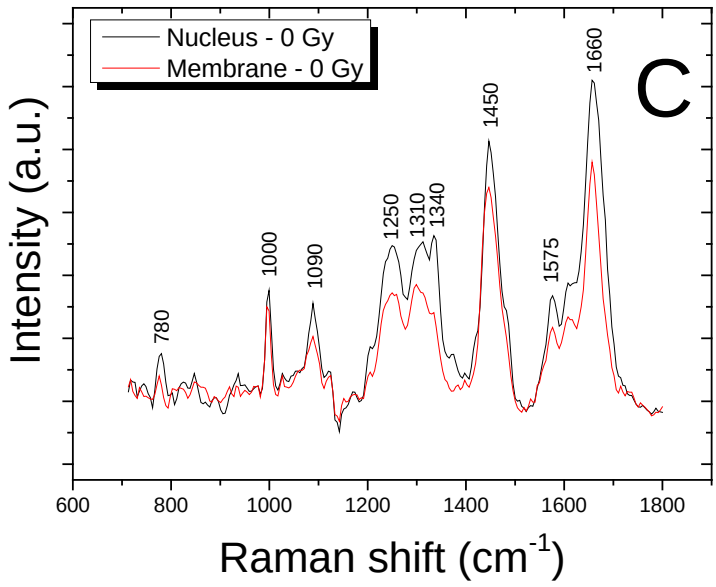

Fig. 1. Average spectra (lines a) of the control samples for the nucleus (A) and the membrane (B), fixed immediately after irradiation (0 Gy; t = 0 h), in the 700-1800 cm^{-1} range, with deconvolution analysis of peaks with Lorentzian curves (lines b) and fit residuals (c). Direct comparison between the two average spectra (C). Main peaks are labelled.

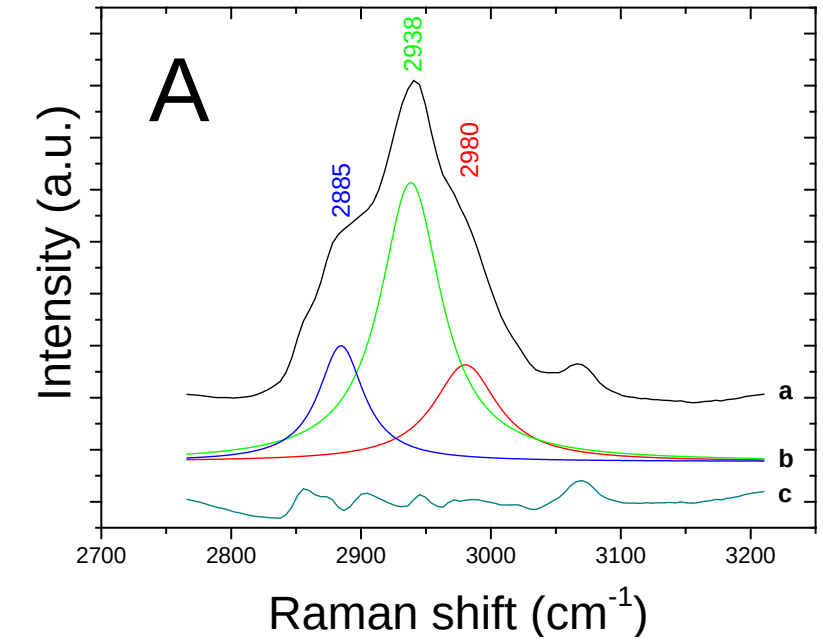
A
2938
2980
2885
Intensity (a.u.)
a
b
c
2700
2800
2900
3000
3100
3200
Raman shift (cm-1)

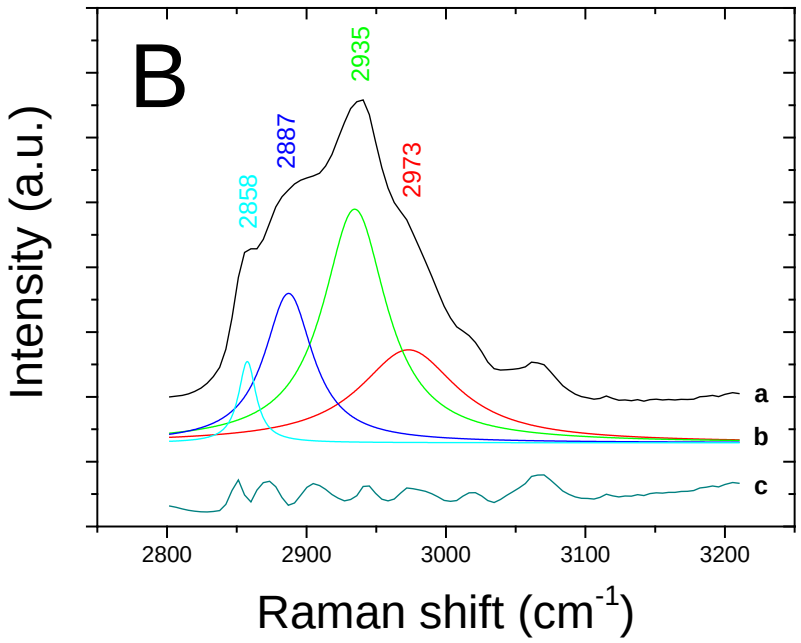
B
2935
2887
2858
2973
Intensity (a.u.)
a
b
c
2800
2900
3000
3100
3200
Raman shift (cm-1)

Fig. 2 (cont'd)

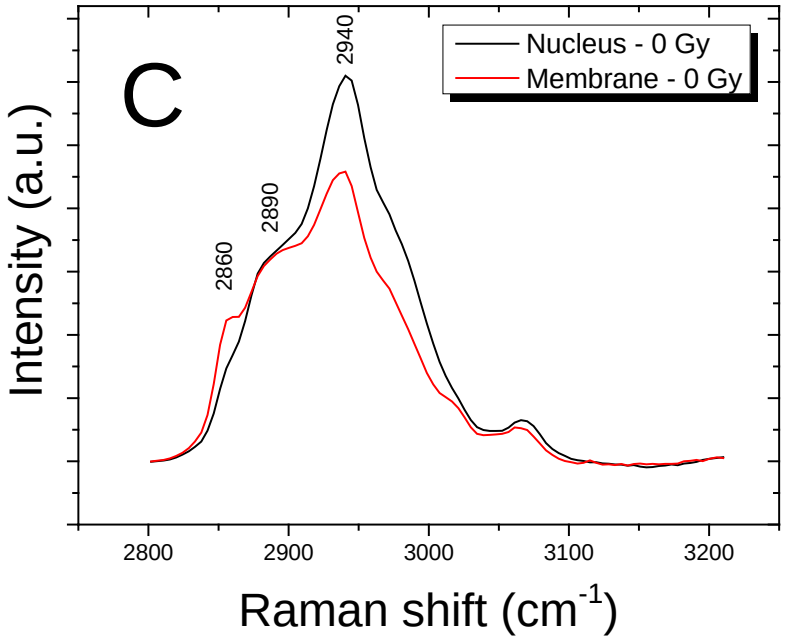

Fig. 2. Average spectra (lines a) of the control samples for the nucleus (A) and the membrane (B), fixed immediately after irradiation (0 Gy; t = 0 h), in the 2800-3200 cm^{-1} range, with deconvolution analysis of peaks with Lorentzian curves (lines b) and fit residuals (c). Direct comparison between the two average spectra (C). Main peaks are labeled

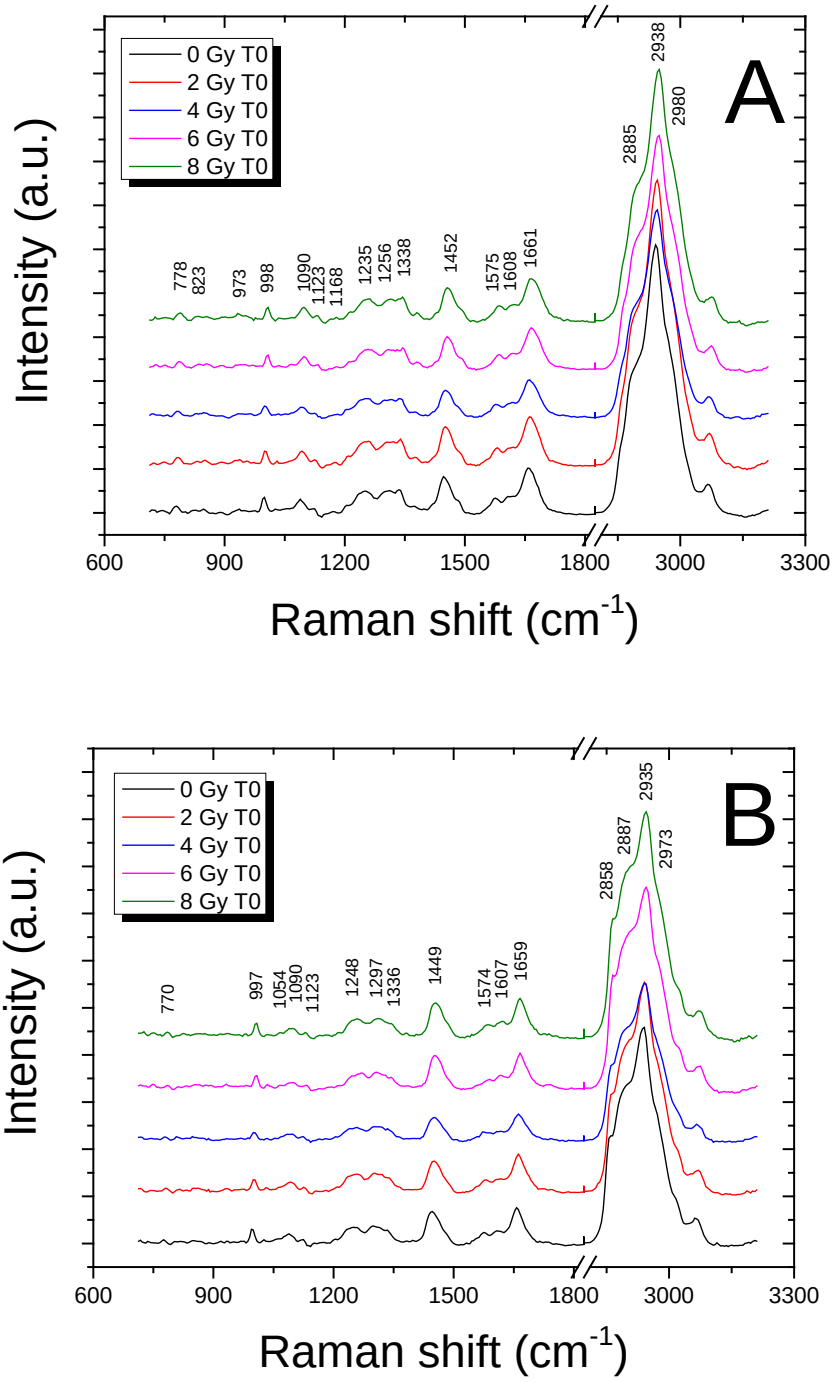

Fig. 3. Comparison of average Raman spectra of the control cells (0 Gy; t = 0 h) and irradiated cells (2; 4; 6; 8 Gy; t = 0 h) for nucleus (A) and membrane (B) region; the spectra are shifted in intensity to allow the comparison and present a break in free peaks; principal peak position, for the control sample are indicated.

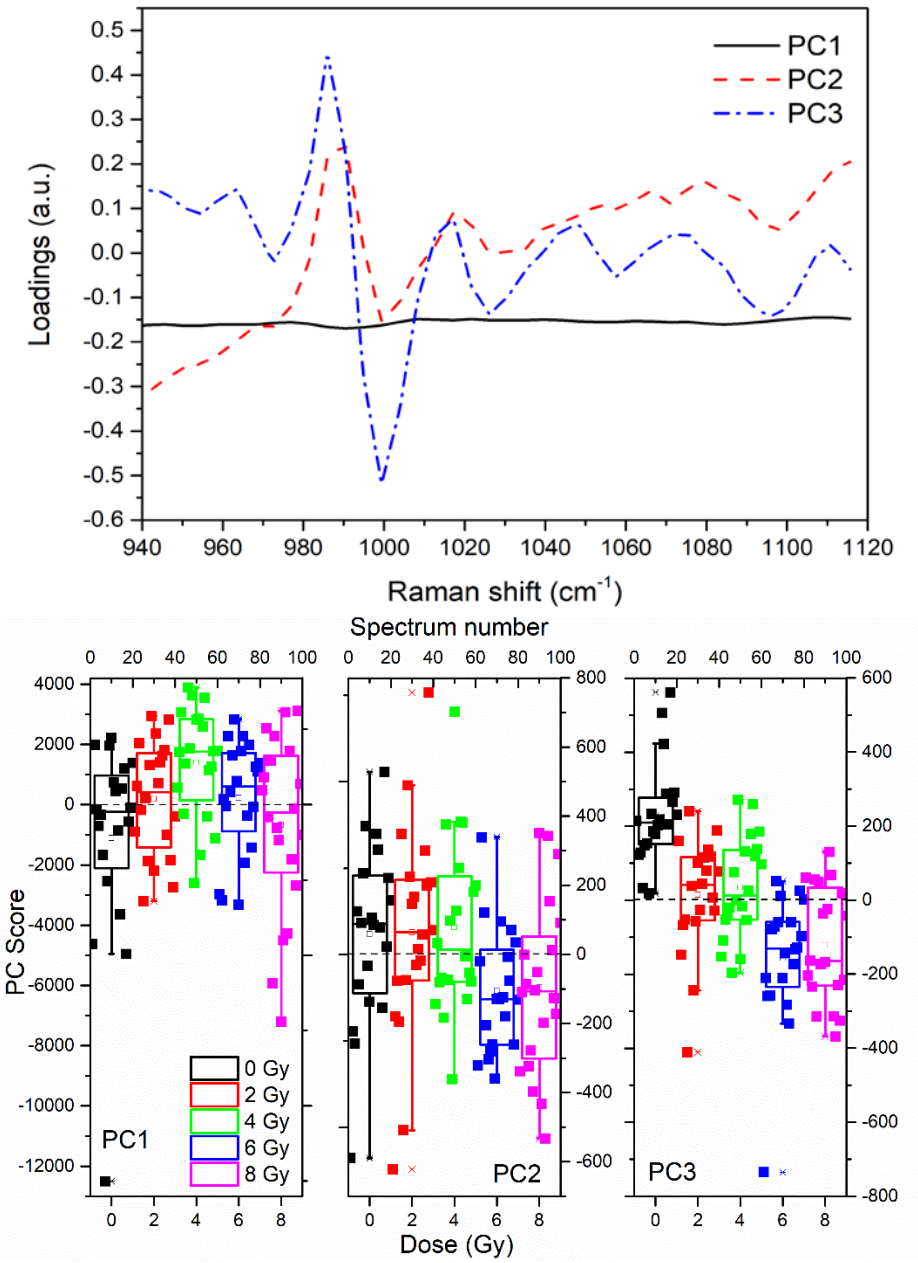

Fig. 4. Results of i-PCA analysis of spectra from the membrane of t0-cells: outcomes for the 933-1115 cm^{-1} spectral region. Upper panel: the first three eigenvectors (PCs). Lower panels: PC1, PC2 and PC3 score plots along with the box plots representation of the data separately evaluated for each "irradiation treatment", i.e, 0 Gy, 2 Gy, 4 Gy, 6 Gy and 8 Gy of irradiation dose.

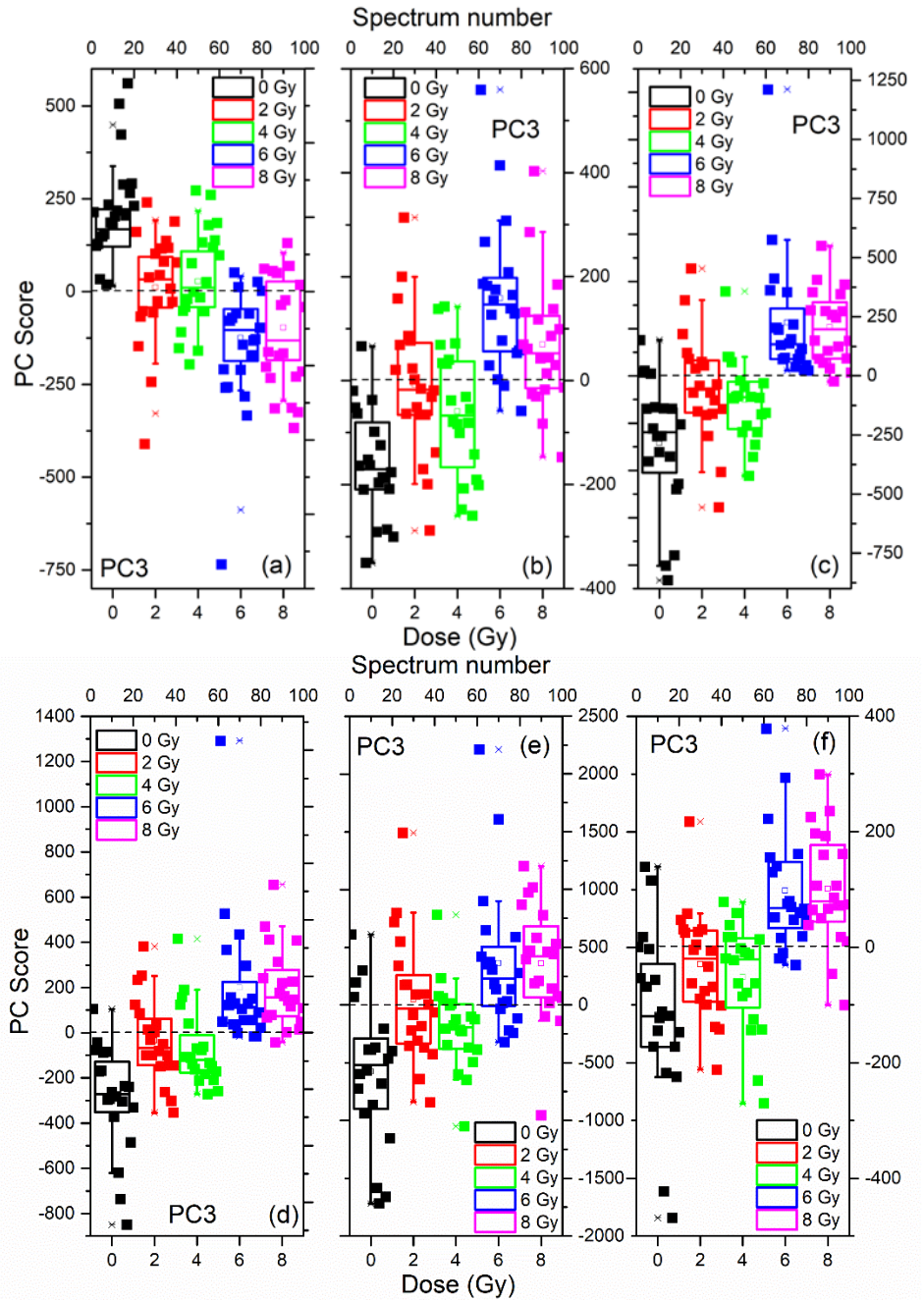

Fig. 5. i-PCA score values results for membrane-related t0-cells spectra. Score plots along with the box plots representation of the data separately evaluated for each "irradiation treatment", i.e, 0 Gy, 2 Gy, 4 Gy, 6 Gy and 8 Gy of irradiation dose (right), for the PCs showing a dependence on the dose for the following spectral ranges (intervals and considered component): (a) 933-1115 cm^{-1}, PC3; (b) 1116-1281 cm^{-1}, PC3; (c) 1407-1532 cm^{-1}, PC3; (d) 1586-1715 cm^{-1}, PC3; (e) 2909-3030 cm^{-1}, PC3; (f) 3031-3100 cm^{-1}, PC3 (see text).

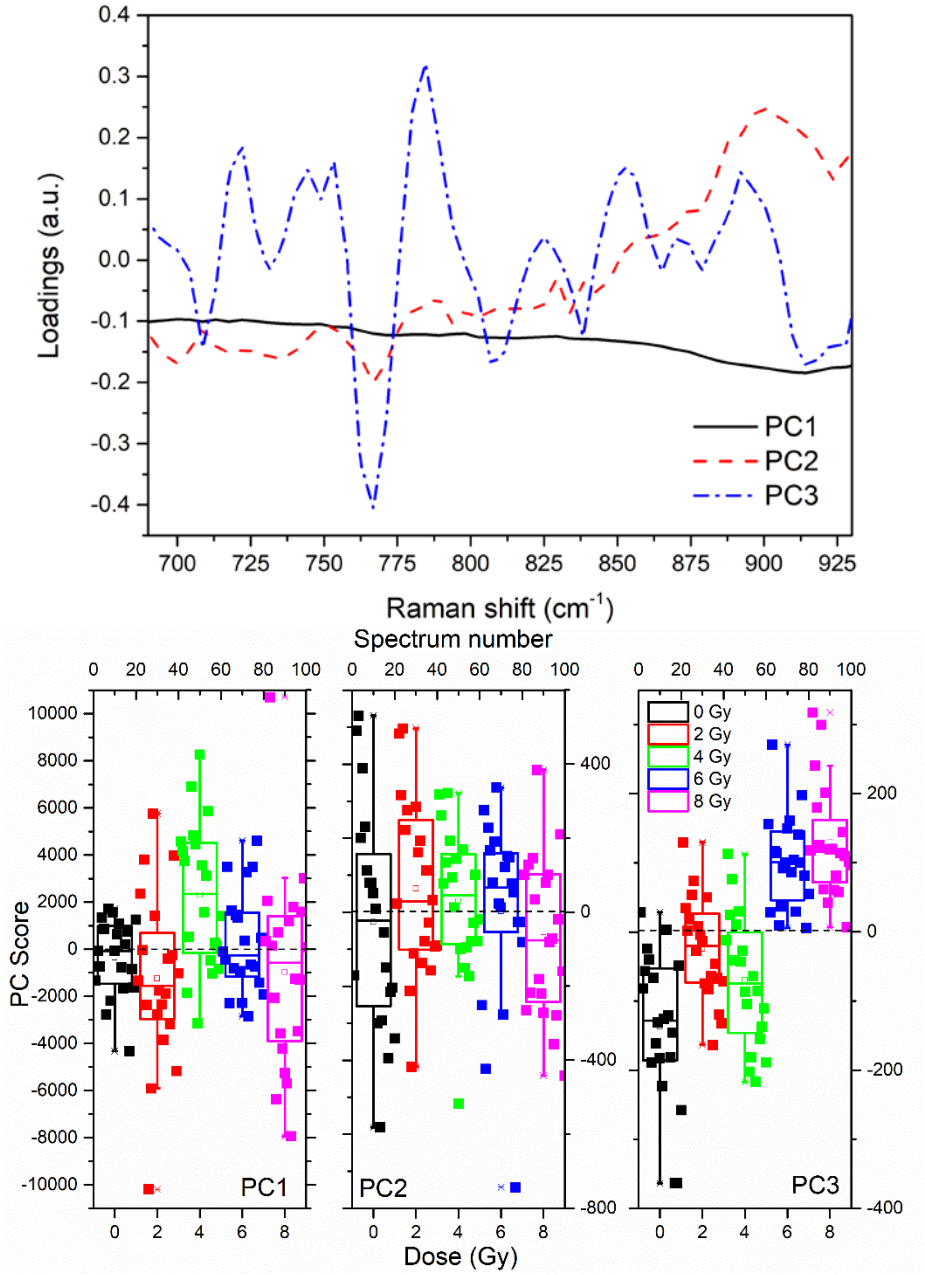

Fig. 6. Results of i-PCA analysis of spectra from the nucleus of t0-cells: outcomes for the 686-932 cm^{-1} spectral region. Upper panel: the first three eigenvectors (PCs). Lower panels: PC1, PC2 and PC3 score plots along with the box plots representation of the data separately evaluated for each "irradiation treatment", i.e, 0 Gy, 2 Gy, 4 Gy, 6 Gy and 8 Gy of irradiation dose.

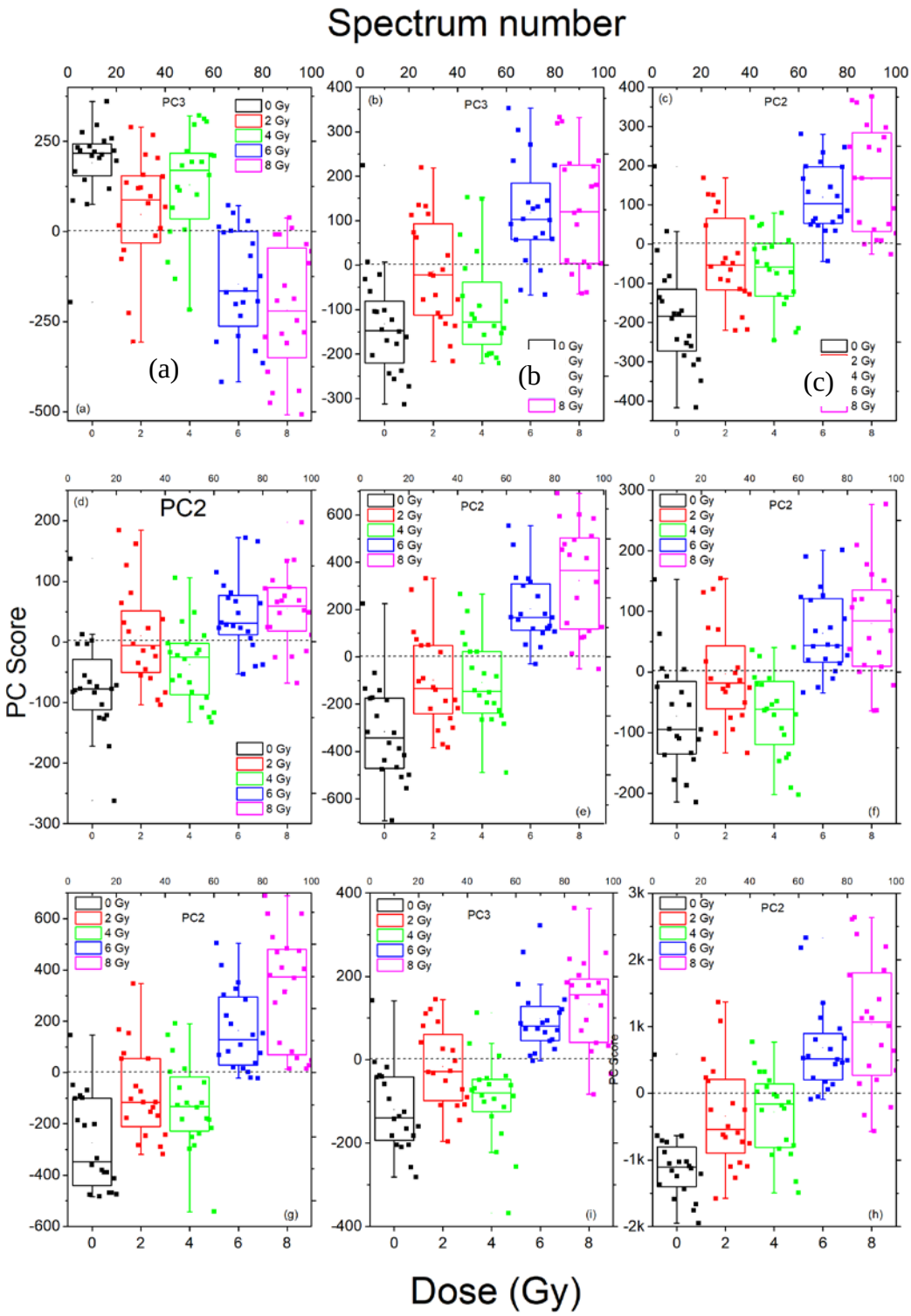

Fig. 7. i-PCA score values results for nucleus-related t0-cells spectra. Score plots along with the box plots representation of the data separately evaluated for each "irradiation treatment", i.e, 0 Gy, 2 Gy, 4 Gy, 6 Gy and 8 Gy of irradiation dose (right), for the PCs showing a dependence on the dose for the following spectral ranges (intervals and considered component): (a) 933-1115 cm^{-1}, PC3; (b) 1116-1281 cm^{-1}, PC3; (c) 1282-1357 cm^{-1}, PC2; (d) 1358-1406 cm^{-1}, PC2; (e) 1407-1532 cm^{-1}, PC2; (f) 1533-1585 cm^{-1}, PC2; (g) 1586-1715 cm^{-1}, PC2; (h) 2909-3030 cm^{-1}, PC2; (i) 3031-3100 cm^{-1}, PC3 (see text).

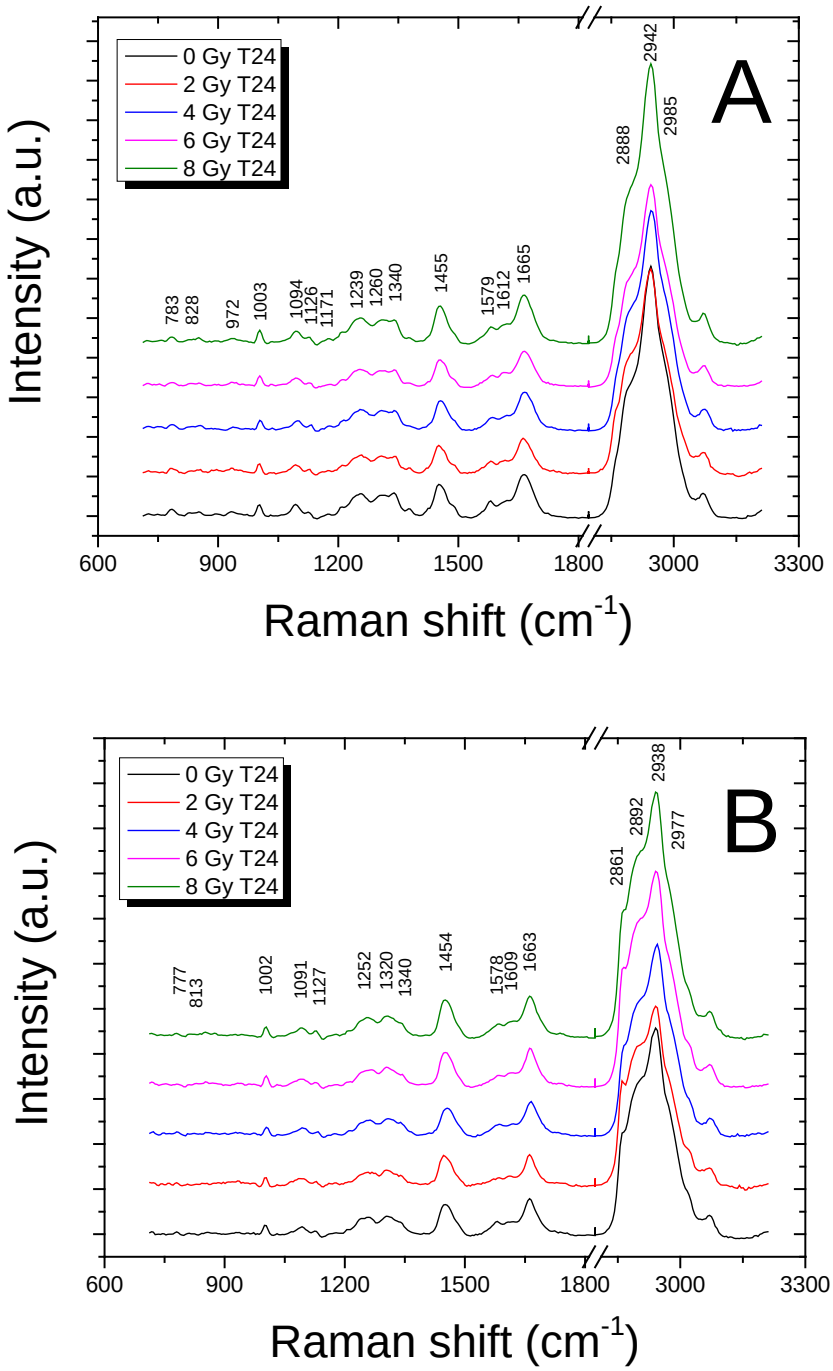

Fig. 8. Comparison of average Raman spectra of the non-irradiated (0 Gy; t = 24 h) and irradiated cells (2; 4; 6; 8 Gy; t = 24 h) for nucleus (A) and membrane (B); the spectra are shifted in intensity to allow the comparison and present a break in free peaks region [1800 - 2800 cm^{-1}]; principal peak position, for the non-irradiated sample are indicated.

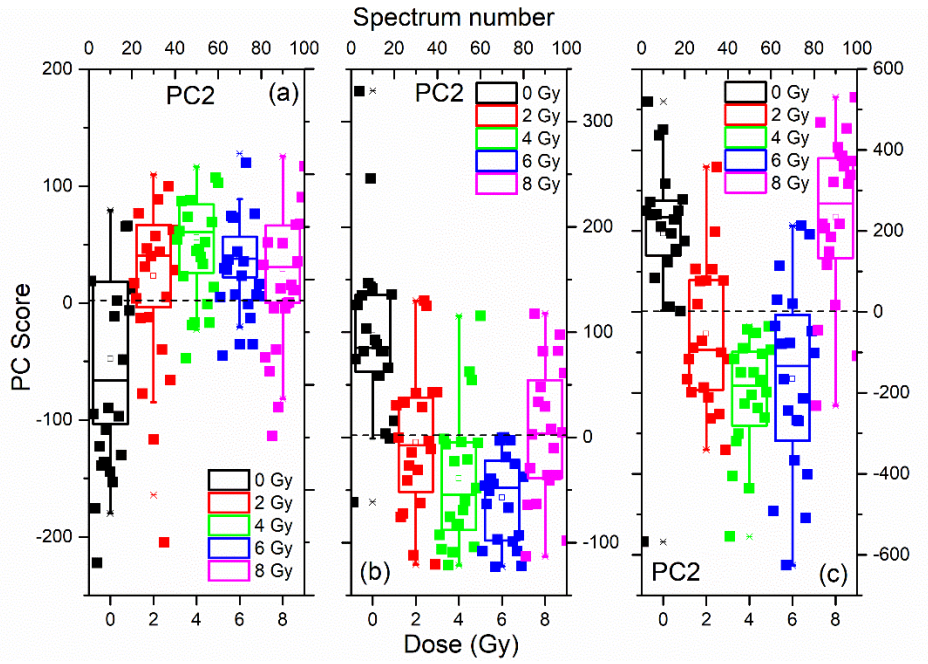

Fig. 9. i-PCA score values results for nucleus-related t24-cells spectra. Score plots along with the box plots representation of the data separately evaluated for each "irradiation treatment", i.e, 0 Gy, 2 Gy, 4 Gy, 6 Gy and 8 Gy of irradiation dose (right), for the PCs showing a dependence on the dose for the following spectral ranges (intervals and considered component): (a) 1358-1406 cm^{-1}, PC2; (b) 1533-1585 cm^{-1}, PC2; (c) 1586-1715 cm^{-1}, PC2 (see text).

Table 1. Raman peak positions and shift for the investigated irradiation doses compared to the control sample, for the **cell membrane region** of samples fixed immediately after irradiation (t0 samples). The shift in terms of units of wavenumber are indicated when present in brackets (bold characters stand for shifts greater than the spectral resolution of the instrument 4 cm^{-1}). Abbreviation: p = protein, l = lipids, c = carbohydrates, d = DNA.

0 Gy	**2 Gy**	**4 Gy**	**6 Gy**	**8 Gy**
Peak position (cm^{-1})	Peak position (shift) (cm^{-1})	Peak position (shift) (cm^{-1})	Peak position (shift) (cm^{-1})	Peak position (shift) (cm^{-1})
2973 (p, l)	2978 (**+5**)	2978 (**+5**)	2977 (+4)	2978 (**+5**)
2935 (p, l)	2938 (+3)	2938 (+3)	2941 (**+6**)	2941 (**+6**)
2887 (l)	2891 (+4)	2890 (+3)	2894 (**+7**)	2894 (**+7**)
2858 (l)	2861 (+3)	2861 (+3)	2865 (**+7**)	2865 (**+7**)
1659 (p, l)	1663 (+4)	1663 (+4)	1667 (**+8**)	1667 (**+8**)
1607 (p)	1610 (+3)	1609 (+2)	1616 (**+9**)	1617 (**+10**)
1574 (d)	1578 (+4)	1577 (+3)	1585 (**+11**)	1584 (**+10**)
1449 (p, l)	1453 (+4)	1453 (+4)	1456 (**+7**)	1457 (**+8**)
1336 (d, p, c)	1340 (+4)	1340 (+4)	1346 (**+10**)	1346 (**+10**)
1315 (d, p, l)	1320 (**+5**)	1318 (+3)	1327 (**+12**)	1325 (**+10**)
1297 (l)	1301 (+4)	1300 (+3)	1307 (**+10**)	1306 (**+9**)
1248 (d, p)	1252 (+4)	1251 (+3)	1261 (**+13**)	1256 (**+8**)
1123 (p, l, c)	unresolved	unresolved	unresolved	1130 (**+7**)
1090 (d, l, c)	1094 (+4)	1090	1095 (**+5**)	1095 (**+6**)
1054 (d,p,l)	unresolved	unresolved	unresolved	1065 (**+9**)
997 (p)	1002 (**+5**)	1002 (**+5**)	1006 (**+9**)	1007 (**+10**)
938 (p, c)	933 (**-5**)	unresolved	944 (**+6**)	937 (-1)
854 (p)	857 (+3)	850 (-4)	855 (+1)	864 (**+10**)
814 (d, l)	unresolved	809 (**-5**)	unresolved	824 (**+10**)
770 (d)	782 (**+12**)	778 (**+8**)	784 (**+14**)	783 (**+13**)

Table 2. Raman peak positions and shifts for the investigated irradiation doses compared to the control sample, for the **cell nucleus region** of samples fixed immediately after irradiation (t0 samples). The shift in terms of units of wavenumber are indicated when present in brackets (bold characters stand for shifts greater than the spectral resolution of the instrument 4 cm^{-1}). Abbreviation: p = protein, l = lipids, c = carbohydrates, d = DNA.

0 Gy	**2 Gy**	**4 Gy**	**6 Gy**	**8 Gy**
Peak position (cm^{-1})	Peak position (shift) (cm^{-1})	Peak position (shift) (cm^{-1})	Peak position (shift) (cm^{-1})	Peak position (shift) (cm^{-1})
2980 (p, l)	2982 (+2)	2984 (+4)	2988 (**+8**)	2989 (**+9**)
2938 (p, l)	2941 (+3)	2941 (+3)	2945 (**+7**)	2946 (**+8**)
2885 (l)	2888 (+3)	2887 (+2)	2891 (**+6**)	2892 (**+7**)
1661 (p, l)	1664 (+3)	1664 (+3)	1668 (**+7**)	1669 (**+8**)
1608 (p)	1611 (+3)	1610 (+2)	1616 (**+8**)	1616 (**+8**)
1575 (d)	1578 (+3)	1577 (+2)	1583 (**+8**)	1584 (**+9**)
1452 (p, l)	1455 (+3)	1454 (+2)	1459 (**+7**)	1459 (**+7**)
1338 (d, p, c)	1341 (+3)	1340 (+2)	1346 (**+8**)	1345 (**+7**)
1309 (d, p, l)	1309	1308 (-1)	1315 (**+6**)	1312 (+3)
1256 (p)	1261 (**+5**)	1259 (+3)	1267 (**+11**)	1262 (**+6**)
1235 (p)	1241 (**+6**)	1237 (+2)	1245 (**+10**)	1241 (**+6**)
1204 (p)	1207 (+3)	1204	1211 (**+7**)	1212 (**+8**)
1168 (p)	1171 (+3)	1172 (+4)	1175 (**+7**)	1174 (**+6**)
1123 (p, l, c)	1126 (+3)	1125 (+2)	1131 (**+8**)	1121 (-2)
1090 (d, l, c)	1094 (+4)	1093 (+3)	1098 (**+8**)	1098 (**+8**)
1051 (d, p, l)	1057 (**+6**)	1055 (+4)	1065 (**+14**)	1049 (-2)
1027 (p)	1030 (+3)	1033 (**+6**)	1036 (**+9**)	unresolved
998 (p)	1002 (+4)	1001 (+3)	1007 (**+9**)	787 (**+9**)
973 (d, p, l)	973	963 (**-10**)	973	unresolved
955 (l)	956 (+1)	944 (**-11**)	943 (**-12**)	951 (-4)
932 (p, c)	933 (+1)	931 (-1)	928 (-4)	933 (+1)
886 (d, l, c)	891 (**+5**)	892 (**+6**)	892 (**+6**)	898 (**+12**)
849 (p)	852 (+3)	845 (-4)	857 (**+8**)	855 (**+6**)
823 (d, p)	829 (**+6**)	unresolved	834 (**+11**)	832 (**+9**)
778 (d)	783 (**+5**)	782 (+4)	787 (**+9**)	787 (**+9**)

Table 3. Synopsis of i-PCA results for intervals showing one PC with dose dependent score for spectra from **membrane** region, t = 0 fixed cells. The negative features are reported using bold characters. The explained variability is reported for the selected components for each interval. Abbreviation: pos.=position

T = 0 Fixed cells	**933-1115 cm^{-1} (PC3: 0.60%)**	**1116-1281 cm^{-1} (PC3: 0.50%)**	**1407-1532 cm^{-1} (PC3: 1.6 %)**	**1586-1715 cm^{-1} (PC3: 1.4%)**	**2909-3030 cm^{-1} (PC3: 0.73%)**	**3031-3100 cm^{-1} (PC3: 0.32%)**
DNA/ RNA features (pos. in cm^{-1})	986, **1058**, **1098**		1487			
Protein features (pos. in cm^{-1})	986, **1000**, **1026**	1125, **1169**, 1178, **1192**, **1219**, 1259	1460	1600, 1621, **1661**	**2918**, 2950, 2972	
Lipid/carbohydrate features (pos. in cm^{-1})	963, 986, **1058**, **1098**	1125, 1259	1460	**1661**	**2918**, 2950, 2972, **3008**	**3057**
Score vs Dose	Decrease from (+) to (-) values (change sign at 6 Gy)	Increase from (-) to (+) values (change sign at 6 Gy)				

Table 4. Synopsis of i-PCA results for intervals showing one PC with dose dependent score for spectra from **nucleus** region- t = 0 fixed cells. The negative features are reported using bold characters. The explained variability is reported for the selected components for each interval. Abbreviation: pos.=position.

T = 0 Fixed cells	**686-932 cm^{-1} (PC3:0.16 %)**	**933-1115 cm^{-1} (PC3: 0.61%)**	**1116-1281 cm^{-1} (PC3: 0.60%)**	**1282-1357 cm^{-1} (PC2: 1.4%)**	**1358-1406 cm^{-1} (PC2: 0.70%)**	**1407-1532 cm^{-1} (PC2: 3.3 %)**	**1533-1585 cm^{-1} (PC2: 1.2 %)**	**1586-1715 cm^{-1} (PC2: 2.8%)**	**2909-3030 cm^{-1} (PC2: 3.5%)**	**3031-3100 cm^{-1} (PC3: 0.41%)**
DNA/ RNA features (pos. in cm^{-1})	722, 784, **811**, 824	986, **1058**, **1098**		**1326**, 1340	1375	**1430** 1487	1581			
Protein features (pos. in cm^{-1})	**766**, 824, **838**, 851	940, 986, **1000**, **1026**	1125, 1174, **1192**, **1219**, 1263	**1326**, 1340		1460		**1594**, **1640**, 1670	**2918**, 2950	
Lipid/carbohydrate features (pos. in cm^{-1})	**708**, 722, 874	940, 963, 986, **1058**, **1098**	1125, 1263			1460		1670	**2918**, 2950, 2994	**3057**
Score vs Dose	Increase from (-) to (+) values (change sign at 6 Gy)	Decrease from (+) to (-) values (change sign at 6 Gy)	Increase from (-) to (+) values (change sign at 6 Gy)							

Table 5. Raman peak position and shifts for the investigated irradiation doses compared to the control sample, for the **cell membrane region** of samples fixed 24 h after irradiation (t24h samples). The shift in terms of units of wavenumber are indicated when present in brackets (bold characters stand for shifts greater than the spectral resolution of the instrument 4 cm^{-1}). Abbreviation: p = protein, l = lipids, c = carbohydrates, d = DNA.

0 Gy	**2 Gy**	**4 Gy**	**6 Gy**	**8 Gy**
Peak position (cm^{-1})	Peak position (shift) (cm^{-1})	Peak position (shift) (cm^{-1})	Peak position (shift) (cm^{-1})	Peak position (shift) (cm^{-1})
2977 (p, l)	2976 (-1)	2983 (**+6**)	2979 (+2)	2977
2938 (p, l)	2938	2941 (+3)	2939 (+1)	2939 (+1)
2892 (l)	2891 (-1)	2894 (+2)	2893 (+1)	2892
2861 (l)	2861	2865 (+4)	2863 (+2)	2862 (+1)
1663 (p, l)	1663	1666 (+3)	1664 (+1)	1664 (+1)
1609 (p)	1611 (+2)	1614 (**+5**)	1613 (+4)	1612 (+3)
1578 (d)	1579 (+1)	1582 (+4)	1581 (+3)	1580 (+2)
1454 (p, l)	1452 (-2)	1457 (+3)	1454	1454
1340 (d, p, c)	1342 (+2)	1342 (+2)	1344 (+4)	1342 (+2)
1303 (d, p, l)	1306 (+3)	1305 (+2)	1304 (+1)	1303
1252 (d, p)	1256 (+4)	1256 (+4)	1256 (+4)	1254 (+2)
1127 (p, l, c)	1129 (+2)	1132 (**+5**)	1129(+2)	1128 (+1)
1091 (d, l, c)	1089 (-2)	1093 (+2)	1090 (-1)	1090 (-1)
1002 (p)	1002	1005 (+3)	1004 (+2)	1003 (+1)
936 (p, c)	931 (**-5**)	935 (-1)	936	939 (+3)
878 (d)	881 (+3)	unresolved	974 (-4)	unresolved
856 (p)	847 (**-9**)	855 (-1)	853 (-3)	854 (-2)
813 (d, l)	824 (**+11**)	unresolved	828 (**+15**)	814 (+1)
777 (d)	765 (**-12**)	779 (+2)	777	777

Table 6. Raman peak position and shifts for the investigated irradiation doses compared to the control sample, for the **cell nucleus region** of samples fixed 24 h after irradiation (t24h samples). The shift in terms of units of wavenumber are indicated when present in brackets (bold characters stand for shifts greater than the spectral resolution of the instrument 4 cm^{-1}). Abbreviation: p=protein, l=lipids, c=carbohydrates, d=DNA.

0 Gy	**2 Gy**	**4 Gy**	**6 Gy**	**8 Gy**	**10 Gy**
Peak position (cm^{-1})	Peak position (shift) (cm^{-1})	Peak position (shift) (cm^{-1})	Peak position (shift) (cm^{-1})	Peak position (shift) (cm^{-1})	Peak position (cm^{-1})
2985 (p, l)	2983 (-2)	2988 (+3)	2987 (+2)	2986 (+1)	2983 (-2)
2942 (p, l)	2942	2945 (+3)	2943 (+1)	2943 (+1)	2940 (-2)
2888 (l)	2888	2890 (+2)	2889 (+1)	2889 (+1)	2887 (-1)
1665 (p, l)	1664 (-1)	1667 (+2)	1666 (+1)	1665	1664 (-1)
1612 (p)	1611 (-1)	1615 (+3)	1613 (+1)	1612	1610 (-2)
1579 (d)	1579	1583 (+4)	1581 (+2)	1580 (+1)	1577 (-2)
1455 (p, l)	1455	1458 (+3)	1457 (+2)	1456 (+1)	1454 (-1)
1340 (d, p, c)	1341 (+1)	1343 (+3)	1341 (+1)	1341 (+1)	1339 (-1)
1307 (d, p, l)	1309 (+2)	1310 (+3)	1309 (+2)	1310 (+3)	1308 (+1)
1260 (p, l)	1258 (-2)	1261 (+1)	1262 (+2)	1260	1259 (-1)
1239 (p)	1236 (-3)	1239	1240 (+1)	1238 (-1)	1236 (-3)
1207 (p)	1208 (+1)	1211 (+4)	1208 (+1)	1208 (+1)	1207
1171 (p)	1171	1175 (+4)	1172 (+1)	1172 (+1)	1169 (-2)
1126 (p, l, c)	1128 (+2)	1132 (**+6**)	1130 (+4)	1128 (+2)	1127 (+1)
1094 (d, p, l)	1094	1098 (+4)	1095 (+1)	1095 (+1)	1093 (-1)
1053 (d, l, c)	1059 (**+6**)	1064 (+**11**)	1055 (+2)	1050 (-3)	unresolved
1032 (p)	1033 (+1)	1035 (+3)	1033 (+1)	unresolved	1043 (**+11**)
1003 (p)	1003	1008 (**+5**)	1004 (+1)	1004 (+1)	1001 (-2)
972 (d, p, l)	973 (+1)	973 (+1)	971 (-1)	970 (-2)	968 (-4)
955 (l)	956 (+1)	unresolved	unresolved	unresolved	Unresolved
933 (p, c)	934 (+1)	939 (**+6**)	unresolved	936 (+3)	938 (**+5**)
895 (d, l, c)	893 (-2)	891 (-4)	892 (-3)	unresolved	888 (**-7**)
852 (p)	852	855 (+3)	853 (+1)	849 (-3)	848 (-4)
828 (d, p)	830 (+2)	830 (+2)	830 (+2)	824 (-4)	823 (**-5**)
783 (d)	785 (+2)	783	783	782 (-1)	777 (**-6**)

Table 7. Synopsis of i-PCA results for intervals showing one PC with dose dependent score for spectra from **nucleus** region- t = 24h-fixed cells. The negative features are reported using bold characters. The explained variability is reported for the selected components for each interval. Abbreviation: pos.=position.

T = 24h Fixed cells	**1358-1406 cm^{-1} (PC2: 0.74%)**	**1533-1585 cm^{-1} (PC2: 1.12 %)**	**1586-1715 cm^{-1} (PC2: 2.8%)**
DNA/ RNA features (pos. in cm^{-1})	**1371**	1572	
Protein features (pos. in cm^{-1})			1648
Lipid features (pos. in cm^{-1})			1648
Score behavior vs Dose	Increase from (-) to (+) values (change sign 2Gy significant within errors 4Gy)	Non monotonus behaviour	Increase from (-) to (+) values (change sign 2Gy significant within errors 4Gy) 8Gy positive